Bulletin of Earthquake Engineering
https://doi.org/10.1007/s10518-026-02419-7

ORIGINAL ARTICLE

Ground response analysis and liquefaction assessment of subsea soils at an offshore platform site

Hyejin Lee[1,2] · Byungmin Kim[3] · Jieun Kim[3] · Taek Hee Han[1] · Jun Kil Park[1] · Youngjin Choi[1] · Hyung-Ik Cho[4] · Jae-Hyun Kim[5] · Jeongmin Goo[6]

Received: 18 July 2025 / Accepted: 26 February 2026

Abstract
The development of underwater infrastructure is increasingly important due to the rising demand for offshore resource utilization and marine spatial expansion. This study evaluates the seismic behavior of subsea soil at a proposed offshore platform site, focusing on liquefaction potential and cyclic softening. Site-specific geotechnical investigations, including Standard penetration tests (SPT), cone penetration tests (CPT), and shear wave velocity (V_S) measurements, were conducted to characterize the soil profile. Nonlinear site response analysis revealed significant amplification of seismic waves in the 0.2–2.0 s period range, due to soft clay layers. Liquefaction potential was evaluated using cyclic resistance ratio (CRR) and cyclic stress ratio (CSR) methods, following KDS 17 10 00 and effective stress-based dynamic analysis. Results indicated that the upper soil layers consist of high-plasticity clay, have a low likelihood of liquefaction. Cyclic softening analysis showed that softening may occur at shallow depths under 50-year return period earthquakes, and more broadly under 500-year events. The factor of safety varied depending on the undrained shear strength (S_u) estimation method. While the site satisfies international seismic design standards for liquefaction, potential cyclic softening suggests that further design considerations are needed. This study offers a practical framework for evaluating seismic stability of submarine soils.

Keywords Seismic site response · Cyclic softening · Marine structure · Offshore foundation · Submarine soils · Site investigation

1 Introduction

The excessive utilization and progressive environmental degradation of terrestrial spaces have underscored the necessity of exploring alternative domains for sustainable development. Among these, marine space has emerged as a key area of interest due to its potential for natural resource exploitation and strategic military significance. Globally, numerous initiatives are being pursued to expand territorial opportunities through the construction of undersea bases and even underwater cities, aimed at utilizing and securing seabed resources

Extended author information available on the last page of the article

Published online: 17 March 2026

(Han et al. 2013). For instance, Aquarius, located 19 m beneath the seabed near Florida, USA, serves as a prominent undersea research platform supporting studies in marine biology and chemistry (National Oceanic and Atmospheric Administration (NOAA) 2025). Similarly, Microsoft developed an underwater data center that capitalizes on the thermal advantages of the ocean for efficient cooling (Microsoft 2025).

In South Korea, the demand for underwater space development has been recognized, however, progress has been constrained by technological limitations and challenges in securing investment. Underwater living spaces, in particular, have faced slow progress due to technical uncertainties, safety concerns, and financial risks associated with human habitation and financial uncertainty. A research project is currently underway in South Korea to develop an underwater space at a depth of 30 m, intended to accommodate various facilities, including data centers (Han et al. 2013, 2021). Achieving this requires ensuring the structural stability of the platform and developing a robust foundation system for safe installation and load bearing.

Subsea foundation systems play a crucial role in ensuring the stability of subsea structures by anchoring them to the seabed and enabling them to reliably support various loads. Unlike onshore structures, subsea structures are constantly exposed to dynamic environmental loads such as waves, tides, earthquakes, and currents, which are transmitted to the foundation of structure (Venkataramana and Kawano 1995; Jeng 2015; Huang and Han 2020). Consequently, the foundation of a subsea structure must be designed to withstand these complex loads, particularly seismic shaking, which may induce soil deformation or failure.

While liquefaction triggering is widely assessed in seismic design, it may not be the governing mechanism in cohesive marine soils, which are prevalent in offshore environments. In such soils, cyclic softening induced by repeated loading can lead to progressive strength degradation and cumulative deformation, even when conventional liquefaction criteria indicate stable conditions. However, cyclic softening is not explicitly addressed in most design standards and is rarely quantified in offshore applications. This highlights the need to evaluate both liquefaction and cyclic softening potentials in the seismic assessment of subsea foundations (Shi et al. 2025; Tian and Chen 2021).

This study investigates the liquefaction triggering and cyclic softening potentials of seabed soils at a proposed underwater platform demonstration site located near Sinam-ri, Seosaeng-myeon, Ulju-gun, Ulsan, South Korea. Geotechnical data obtained from standard penetration tests (SPT), cone penetration tests (CPT), and shear wave velocity (V_S) measurements were used to calculate the cyclic resistance ratio (CRR) and cyclic stress ratio (CSR). By comparing these values, this study quantifies the liquefaction susceptibility of site-specific soils under seismic loading conditions. Furthermore, nonlinear site response analysis was conducted to evaluate the dynamic stability of the proposed platform.

While the analytical procedures employed in this study follow established seismic evaluation frameworks, the primary contribution of this work lies in the interpretation of these frameworks when applied to offshore foundation design in cohesive seabed soils. While conventional liquefaction assessments often focus on whether triggering occurs, this study demonstrates that cyclic softening can govern deformation-related performance and serviceability of subsea foundations even when liquefaction is not predicted. By integrating site-specific offshore borehole data with liquefaction and cyclic softening assessments, this study highlights how conventional evaluation results may lead to fundamentally different

design interpretations under increasing seismic demand. The findings therefore provide practical insight into the seismic assessment of offshore foundations at the investigated site, demonstrating that deformation tolerance and sensitivity to seismic input may govern design decisions under cohesive seabed conditions even when conventional liquefaction criteria are satisfied.

2 Study area and site investigation

2.1 Site overview

The research area for this study is located approximately 1.1 km offshore from Shinam-ri, Seosang-myeon, Ulju-gun, Ulsan, South Korea (Fig. 1). The site is in proximity to several major faults, including the Ulsan, Ilsan, Dongnae, and Yangsan faults. They are situated at distances ranging from 5 to 25 km. This region has garnered significant attention due to its seismic activity, notably the 2016 Gyeongju earthquake (**M**5.5) and the 2017 Pohang earthquake (**M**5.4) (Hong et al. 2024; Kang et al. 2019; C. H. Kim et al. 2022a, b). The southeastern portion of the Korean Peninsula has been identified as a primary zone for seismic activity, with magnitudes ranging from 5 to 6 based on instrumental records since 1978. Additionally, the 2017 Pohang earthquake triggered liquefaction in certain areas of South Korea, highlighting the significance of evaluating liquefaction potential in seismic hazard assessments (Ahn et al. 2018; Gihm et al. 2018). Consequently, several studies have been conducted in Korea to investigate liquefaction susceptibility and its implications for geotechnical engineering (Cho et al. 2024; Kim et al. 2021; Seo et al. 2024).

The region also known for its significant historic seismic activity. It is proximate to the site of the July 24, 1643 earthquake near Ulsan, which is considered the largest earthquake ever to have occurred on the Korean Peninsula (Lee 1998). According to the *Historical Earthquake Records in Korea (2~1904)* (Korea Meteorological Administration (KMA)

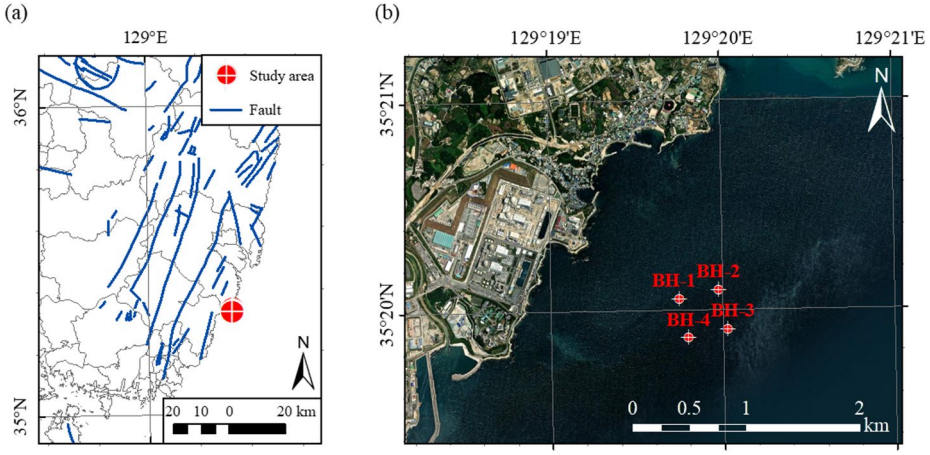

Fig. 1 Study area: (**a**) site location and nearby faults, and (**b**) detatiled aerial view. Fault data retrieved from the Global K-Geoscience Data Hub, Korea Institute of Geoscience and Mineral Resources (KIGAM), http://data.kigam.re.kr/mgeo/, accessed June 2025

2012), the 1643 earthquake is estimated to have had an intensity (I) of 8–9. Historical record describes that "in Ulsan County, the ground cracked, and water gushed out". Using the inverse prediction formula for earthquake magnitude (M) derived from intensity (Seo and Choi 1998):

$$M = 2/3 \times I + 1.0 \tag{1}$$

the magnitude of the 1643 Ulsan earthquake is estimated to range from 6.3 to 7.0.

In addition to historical records, recent studies also highlight the seismic potential of the area. Kyung (2010) reported that earthquakes with a maximum magnitude of 6.8 could occur along the Yugye Fault, part of the Yangsan Fault Zone, and a maximum magnitude of 7.0 along the Galgok Fault, part of the Ulsan Fault Zone. Based on these historical and contemporary studies, the probability of a seismic event reaching a magnitude of 7.0 within the vicinity of the project site is considered reasonable.

2.2 In-situ investigation

The Ulsan region in South Korea frequently experiences small-to-moderate seismic events, necessitating seismic analysis for structures installed on the seabed. The geology of the subject site, based on the geologic map, consists of Cretaceous andesite porphyry, granite, and rhyolite porphyry, unconformably overlain by Quaternary alluvium from the Cenozoic era. Comprehensive site investigations, including borehole logging and sampling, standard penetration tests (SPT), piezocone penetration test (CPTu), and laboratory testing, were carried out at four locations across the study site to characterize the geotechnical properties of ground (Fig. 2). The borehole locations (BH-1 to BH-4) are illustrated in Fig. 1 and summarized in Table 1.

The stratigraphy consists of cohesive soil, sandy soil, weathered soil, and soft rock in descending order from the seabed. The groundwater level at the site corresponds to the sea level. The investigation revealed that the site is predominantly composed of sedimentary clay up to a depth of 30.5 m below the seabed. Below this, a sedimentary sandy soil layer with a thickness ranging from 1 to 9.5 m was identified, underlain by weathered soil and soft rock layers deeper than 9 m. The bedrock, consisting of soft rock, was found to be generally inclined. The depth of bedrock at each borehole was as follows: BH-1, 46.5 m; BH-2, 68 m; BH-3, 78 m; and BH-4, 63 m (Table 1).

BH-1 was identified as the most suitable location for the underwater platform due to its favorable geotechnical properties, including a relatively shallow bedrock and a denser upper sedimentary layer compared to other borehole locations. These conditions provided advantageous foundation support. Consequently, liquefaction potential was primarily evaluated at BH-1 to ensure seismic stability at the selected platform site.

Among the four borehole locations, borehole-based seismic PS logging (hereafter referred to as S-PS logging) was conducted only at BH-2. The S-PS logging was performed using a Mount Sopris Matrix Logger and provided a full vertical V_S profile, as BH-2 penetrated into the underlying bedrock exceeding 50 m. The measured average shear wave velocity of the soil layer was measured at 160 m/s. These data were used to estimate the V_S profile required for site response analysis.

Fig. 2 Overview of borehole investigation activities: (**a**) general overview of drilling operation at BH-1, (**b**) standard penetration test (SPT) at BH-1, (**c**) core sampling at BH-2, and (**d**) S-PS logging at BH-2

Although BH-2 was not selected as the platform location, the availability of high-quality seismic data made it a valuable reference point for evaluating liquefaction potential and dynamic soil behavior. According to the Korean seismic design code (KDS 17 10 00:2024) (KDS 17 10 00 2024), sites with bedrock depths exceeding 50 m are classified as S_6, requiring site-specific seismic hazard evaluations and site response analyses. Similarly, ASCE/SEI 7–22 (American Society of Civil Engineers (ASCE) 2022) standards mandate advanced ground response analyses for sites with deep bedrock or low shear wave velocities (< 180 m/s), categorized as Site Class E or F. Although the classification systems differ, both standards consistently indicate that simplified site classification approaches are not applicable for the studied site. These standards collectively indicate that the geotechnical conditions at BH-2 require careful seismic analysis to ensure structural stability under dynamic loading.

For borehole BH-1, where S-PS logging was not performed, V_S was estimated by applying a site-specific empirical N-V_S correlation developed from measured S-PS logging and SPT-N data in borehole BH-2. BH-2 was selected for S-PS logging as it was the deepest borehole and penetrated into the bedrock layer, providing a full vertical profile. The N-V_S relationship was established using data from borehole BH-2 and subsequently applied to the SPT-N results of BH-1 to generate the shear wave velocity profile. Given the proximity and similarity of the geological formations between BH-1 and BH-2, applying a site-specific

Table 1 Borehole locations, soil layer distribution, and CPT results (q_c,f_s, u_2, and S_u)

Borehole ID	Latitude	Longitude	Cohesive soil depth (m)	Sandy soil depth (m)	Weathered soil depth (m)	Soft rock depth (m)	Total depth (m)	Cone tip resistance (q_c, kPa)	Sleeve friction (f_s, kPa)	Excess pore pressure (u_2, kPa)	Undrained shear strength (S_u, kPa)
BH-1	35°20'03.40"	129°19'44.74"	24.0	11.5	11.0	3.0	49.5	460.3	16.9	732.6	16.1
BH-2	35°20'05.79"	129°19'58.43"	28.5	4.5	35.0	5.0	73.0	520.5	18.0	738.3	16.5
BH-3	35°19'54.57"	129°20'01.35"	30.5	4.0	43.5	-	78.0	448.2	22.5	762.8	12.1
BH-4	35°19'52.18"	129°19'47.66"	25.0	1.0	37.0	3.0	66.0	376.7	23.2	793.5	10.2

correlation derived from BH-2 was deemed more reliable than using generic correlation from other N-V_S equations, whether domestic or international (Kumagai et al. 2020; Kuo et al. 2021; Tsai et al. 2019). The N-V_S correlation was developed using 66 pairs of N and V_S data collected from BH-2, at depths ranging between 2 m and 67 m. The resulting regression equation is as follows:

$$V_S(\mathrm{m/s}) = 2.837 \times N_P + 0.902 \times \mathrm{Depth\,(m)} + 143.463 \tag{2}$$

where N_P represents the corrected N-value for a penetration depth of 30 cm, considering the nonlinear characteristics of penetration resistance. In the weathered soil layer above the soft rock, penetration to a depth of 30 cm is often not achieved even after 50 blows in the SPT. While linear extrapolation of N-value (N_E) is possible in such cases for a penetration depth of 30 cm, this study adopted N_P as a nonlinear correction method, based on recent findings (Sun et al. 2022). Accordingly, the N_P value was determined using the following equations, which are derived from the uncorrected N-value (N_E):

$N_P = N_E + 1.47DP, for DP \leq 15cm$

$$N_P = N_E + 9.61DP - 122.06, for DP > 15cm \tag{3}$$

where DP represents the difference (in cm) between the penetration depth achieved after 50 blows and the standard penetration depth of 30 cm. Using the N_P values as a function of depth, the N-V_S relationship was established for borehole BH-2. This relationship was then applied to the N values from borehole BH-1 to obtain the depth-specific V_S profile, as summarized in Table 2 and illustrated Fig. 3. Nevertheless, uncertainty remains in the estimated V_S profile at BH-1, and this limitation is acknowledged. Moreover, no empirically validated N-V_S models specifically developed for offshore cohesive seabed conditions are currently available. Accordingly, the site-specific correlation derived from in-situ S-PS logging at BH-2 was considered the most appropriate reference for estimating the V_S profile at BH-1, with due recognition of the associated uncertainty.

3 Design ground motion classification and ground motion selection

3.1 Determination of design ground motion

This study was conducted on a nearshore submarine site, as opposed to a typical inland site, and thus, seismic standards applicable to similar environments were also considered. The underwater platform, the structure to be designed, was determined to be seismic category II by applying the seismic design criteria for ports and fishing harbors (KDS 64 17 00:2019) of the Ministry of Oceans and Fisheries (KDS 64 17 00 2019). This classification aligns with the Risk Category II or III as defined in ASCE/SEI 7–22, yet it is designated as Risk Category II because the structure does not serve a critical function under emergency conditions. Instead, its primary function is operational, aligning with the definition provided in ASCE/SEI 7–22 for general structures with moderate importance.

In this study, site response analysis was performed using ground motions corresponding to a 50-year return period (operation level) and a 500-year return period (collapse preven-

tion level), which were classified as seismic performance levels in KDS 17 10 00 and correspond to the service level earthquake (SLE) and design basis earthquake (DBE) in ASCE/SEI 7–22. According to ASCE/SEI 7–22, general building structures are typically designed based on the DBE (475-year return period), while the SLE (50-year return period) is used to evaluate functional performance under moderate seismic conditions. Since the underwater platform in this study is classified as a general structure, the 50-year and 500-year return period seismic levels were selected for the analysis, aligning with both ASCE/SEI 7–22 and KDS 17 10 00 criteria. For the response analysis, effective ground acceleration (S) values of 0.044 g and 0.11 g were adopted based on KDS 17 10 00, considering the 50-year return period (SLE) and the 500-year return period (DBE), respectively. When determining the effective ground acceleration (S) based on administrative zoning methods, it is calculated by multiplying the seismic zone factor (Z) by the hazard coefficient (I) for each mean return period.

To ensure a conservative approach, the Korean National Seismic Hazard Map (National Emergency Management Agency 2013), published in 2013, was examined, providing probabilistic ground motion estimates for different return periods. The selected S values (0.044 g and 0.11 g) exceed the corresponding mapped values of 0.03–0.04 g for the 50-year return period and 0.09–0.1 g for the 500-year return period. Furthermore, ASCE/SEI 7–22 recommends utilizing seismic hazard maps as a basis for determining site-specific ground motion parameters. This approach ensures a comprehensive and reliable evaluation of seismic hazards while maintaining compatibility with both KDS 17 10 00 and ASCE/SEI 7–22 site response methodologies.

Since the effective ground acceleration levels vary between 0.044 g and 0.11 g depending on the service and collapse prevention level, the earthquake magnitude selection criteria for each seismic performance level were classified as follows:

- Service Level Earthquake (S = 0.044 g): $5.0 < \mathbf{M} < 6.0$.
- Design Basis Earthquake (S = 0.11 g): $6.0 < \mathbf{M} < 7.0$.

International seismic design standards, including ASCE/SEI 7–22, Eurocode 8 (Standard 2005), and KDS 17 10 00, require that seismic analysis satisfies the prescribed design response spectrum while also incorporating site-specific characteristics, such as regional fault conditions, through the generation and application of site-specific design ground motions. Accordingly, site-specific design ground motions defined in KDS 17 10 00 were adopted to ensure consistency with national seismic hazard assessments and compliance with international seismic design practices.

3.2 Selection of input ground motion and spectrum matching

The study area is located 5–25 km from major fault zones, including the Ulsan Fault and Yangsan Fault, which are considered potential seismic sources. Based on these criteria, earthquake records were selected with magnitudes ranging from 5.0 to 7.0 and epicentral distances between 5 km and 30 km (Ministry of Construction and Transportation 1997; MOLIT and Korea Authority of Land & Infrastructure Safety 2021). Also, only records obtained under rock outcrop conditions for free-field ground motion recordings were considered to ensure consistency in seismic hazard assessment.

Table 2 Depth-dependent SPT-N values and corresponding measured and predicted shear wave velocities (V_S) for BH-1 and BH-2

Depth (m)	BH-2			BH-1	
	N_E	Measured V_S (m/s)	Predicted V_S (m/s)	N_E	Predicted V_S (m/s)
1	1	143	147.202	1	147.202
2	1	143	148.104	1	148.104
3	1	144	149.006	1	149.006
4	1	148	149.908	1	149.908
5	1	142	150.81	1	150.81
6	1	145	151.712	1	151.712
7	1	146	152.614	1	152.614
8	1	145	153.516	1	153.516
9	1	147	154.418	1	154.418
10	1	149	155.32	1	155.32
11	1	153	156.222	1	156.222
12	1	151	157.124	1	157.124
13	1	155	158.026	1	158.026
14	1	158	158.928	1	158.928
15	1	154	159.83	1	159.83
16	1	153	160.732	1	160.732
17	1	157	161.634	1	161.634
18	1	161	162.536	1	162.536
19	1	160	163.438	1	163.438
20	1	165	164.34	1	164.34
21	1	165	165.242	1	165.242
22	1	165	166.144	1	166.144
23	1	165	167.046	1	167.046
24	1	165	167.948	17	213.34
25	1	165	168.85	19	219.916
26	1	164	169.752	26	240.677
27	1	169	170.654	26	241.579
28	26	174	242.481	24	236.807
29	27	279	246.22	22	232.035
30	27	283	247.122	24	238.611
31	26	284	245.187	22	233.839
32	36	311	274.459	25	243.252
33	42	348	292.383	25	244.154
34	50	373	325.0428	24	242.219
35	50	411	401.8279	29	257.306
36	50	422	430.4139	50	336.2579
37	50	405	391.0515	50	367.909
38	50	416	417.9154	37	282.708
39	50	415	418.8174	50	338.9639
40	50	421	434.0219	50	321.393
41	50	405	394.6595	41	296.762
42	50	411	408.1419	42	300.501
43	50	415	422.4254	50	352.3713
44	50	411	409.9459	50	343.4739
45	50	410	410.8479	50	375.125
46	50	406	399.1695	50	411.7499

Table 2 (continued)

Depth (m)	BH-2			BH-1	
	N_E	Measured V_S (m/s)	Predicted V_S (m/s)	N_E	Predicted V_S (m/s)
47	50	418	426.0334		
48	50	411	413.5539		
49	50	395	378.733		
50	50	400	390.8978		
51	50	415	429.6414		
52	50	404	404.5815		
53	50	412	418.0639		
54	50	415	432.3474		
55	50	389	373.4276		
56	50	396	385.047		
57	50	411	421.6719		
58	50	405	409.9935		
59	50	390	377.0356		
60	50	412	411.7975		
61	50	404	400.8198		
62	50	401	401.7218		
63	50	404	427.0839		
64	50	402	427.9859		
65	50	411	442.2694		
66	50	417	417.2095		
67	-	446	-		
68	-	1184	-		
69	-	1240	-		
70	-	1268	-		
71	-	1257	-		

According to KDS 64 17 00, when performing seismic analysis using actual earthquake records, at least three time-history analyses must be conducted, and the maximum response should be applied. Additionally, the higher-level standard, KDS 17 10 00, specifies that when conducting site response analysis, recorded earthquake motions from intraplate regions similar to Korea's seismic environment should be prioritized. However, it does not explicitly mandate the use of domestic seismic records. Nevertheless, recent studies and seismic performance evaluation guidelines recommend including at least one recorded motion from the 2016 Gyeongju earthquake or the 2017 Pohang earthquake (K. Kim et al. 2022a, b; Ministry of Land and Korea Authority of Land & Infrastructure Safety 2021). In accordance with this recommendation, this study selected three input ground motions for each seismic performance level, including one domestic seismic record, to conduct seismic analysis.

Table 3 summarizes the input ground motions corresponding to the SLE. Among domestically recorded earthquakes, the September 12, 2016 Gyeongju earthquake (**M**5.5) was the largest instrumentally recorded event in South Korea. A portion of its observed records was utilized in this study; however, considering its magnitude, only one record suitable for the service level earthquake was selected. Specifically, the horizontal ground motion recorded at the Myeonggye-ri station (MKL), located approximately 6 km from the epicenter, was obtained from KIGAM Quake (Lee et al. 2024), an online seismic data-sharing

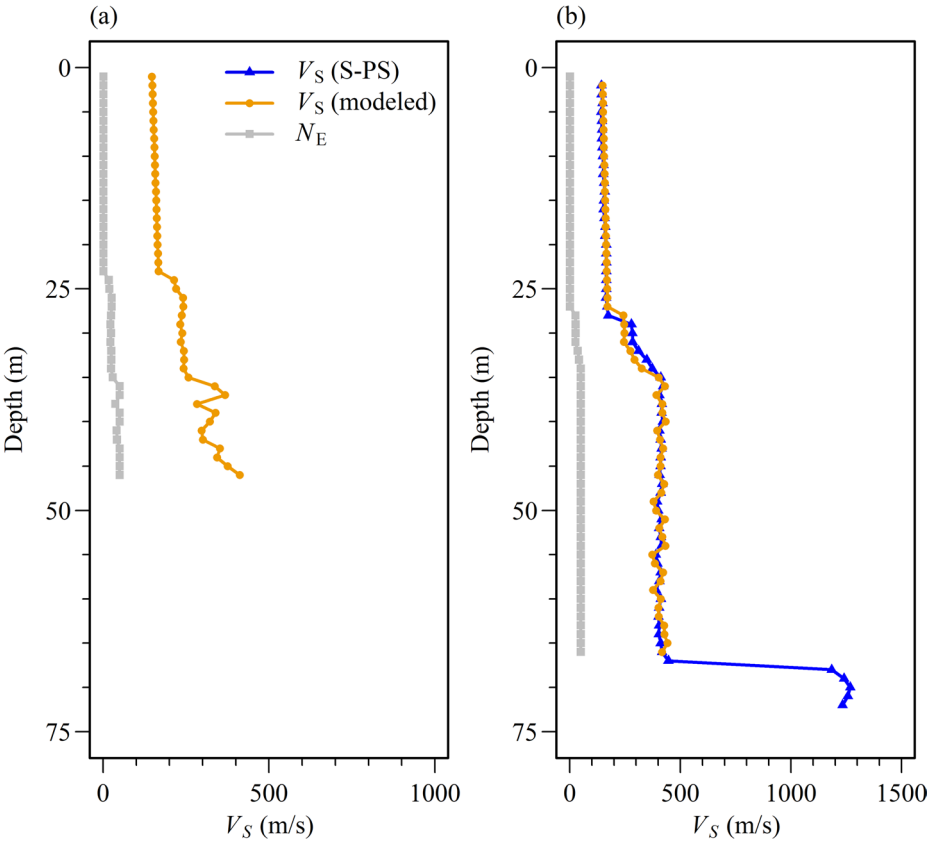

Fig. 3 V_S estimation for BH-1 based on N-V_S relationship from BH-2: (**a**) Estimated V_S profile for BH-1, and (**b**) S-PS data and modeled V_S for BH-2

Table 3 Input ground motion for service level earthquake (SLE)

Database	PEER RSN #	Event	Year	Station	M	R_{jb} (km)	R_{rup} (km)	V_{S30} (m/s)
KIGAM Quake	-	Gyeong-Ju, Korea	2016	MKL	5.5	6 (R_{epi})		860 (Kim et al. 2020)
NGA-East	8571	Mineral, USA	2011	SE.NANPP	5.74	18.5	20.4	554
NGA-West2	146	Coyote Lake, USA	1979	Gilroy Array #1	5.74	10.2	10.7	1,428

Note: R_{jb}: Joyner-Boore distance, which is the shortest horizontal distance from the recording station to the surface projection of the ruptured fault plane. R_{rup}: rupture distance, defined as the closest three-dimensional distance from the recording station to any point on the fault rupture plane

platform operated by the Korea Institute of Geoscience and Mineral Resources (KIGAM). For international earthquake records, the Ground Motion Database of the Pacific Earthquake Engineering Research Center (PEER) was used. To match Korea's intraplate seismic environment, a record from the August 23, 2011 Mineral earthquake in the NGA-East data-

Table 4 Input ground motion for design basis earthquake (DBE)

Database	PEER RSN #	Event	Year	Station	M	R_{jb} (km)	R_{rup} (km)	V_{S30} (m/s)
NGA-West2	1011	Northridge-01, USA	1994	LA - Wonderland Ave	6.69	15.1	20.3	1,223
NGA-West2	4231	Niigata, Japan	2004	NIGH15	6.63	21.8	22.1	686
NGA-West2	5472	Iwate, Japan	2008	AKT017	6.9	31.4	33.8	644

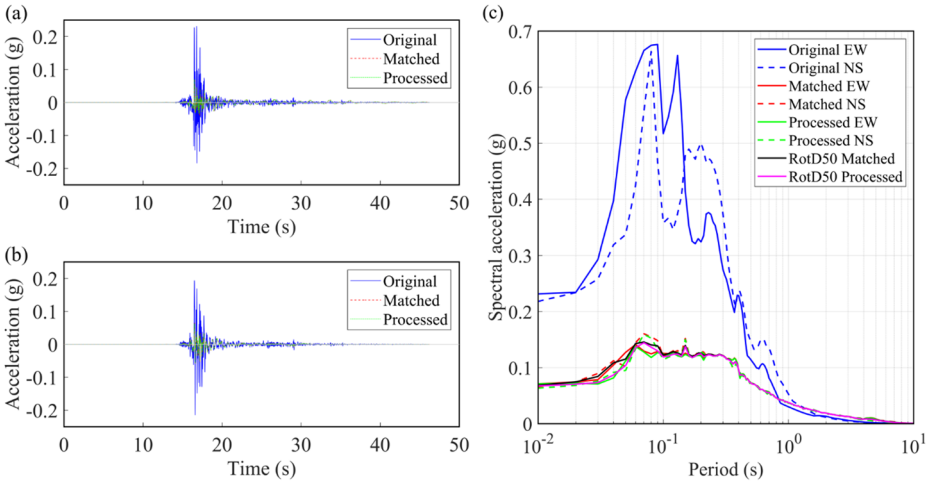

Fig. 4 Acceleration time history and response spectrum before and after spectral matching of the 201 Gyeonju earthquake (MKL station): (**a**) acceleration time history for the EW component, (**b**) acceleration time history for the NS component, and (**c**) response spectra of the original (blue), matched (red), and processed (green) ground motions. RotD50 spectra before and after processing are shown in black and magenta, respectively

base was selected. In addition, a record from the 1979 Coyote Lake earthquake in the NGA-West2 database was used. Table 4 summarizes the input ground motions corresponding to the DBE. The selection of input ground motions for this level was also based on the PEER Ground Motion Database, from which a record of the 1979 Coyote Lake earthquake in the NGA-West2 database was selected.

The SeismoMatch software (2020), which employs the matching algorithm developed by Atik and Abrahamson (2010), was used to adjust the input ground motions to match the standard design response spectrum defined for S1 reference conditions at the rock level. To convert the recorded east-west (EW) and north-south (NS) horizontal ground motion components into a single record, the RotD50 method (Boore 2010) was applied, which computes response spectra for all rotation angles and selects the median spectrum. The mean response spectra of the input ground motions before and after scaling were compared with the standard design response spectrum for S1 soil (Fig. 4). After the scaling process, baseline correction was applied to the adjusted acceleration signals using the methodology proposed by Lee et al. (2018) to derive the matched processed spectrum.

The average 5% damped response spectrum must satisfy at least 90% of the standard design response spectrum within the 0.06–6.0 s period range for S1 soil. Additionally, PGA of the input ground motions must be at least 90% of the S value. To verify compliance,

the 90% threshold of the standard design response spectrum was indicated by a dashed line, and the adjusted acceleration signals were compared against this threshold, confirming compliance with the required criteria. After scaling, the mean PGA of the SLE input ground motions was 0.0577 g (EW) and 0.0644 g (NS), satisfying the required threshold of 90% of S = 0.044 g. Similarly, for the DBE, the mean PGA of the scaled input ground motions was 0.1472 g (EW) and 0.1409 g (NS), exceeding the 90% requirement for S = 0.11 g (Fig. 5).

4 Site response analysis

Nonlinear site response analyses were performed using matched ground motions corresponding to 50-year and 500-year return periods as the input motions. To assess the effects of pore water pressure, both total stress analysis and effective stress analysis were conducted. For effective stress analysis, the Matasovic & Vucetic model (Matasović and Vucetic 1995) was applied to clay layers, while the Green-Mitchell-Polito (GMP) model (Green et al. 2000) was used for sandy layers to account for the pore pressure buildup under cyclic loading. Additionally, the Dobry and Vucetic model (Vucetic and Dobry 1986) and the Park and Ahn model (Park and Ahn 2013) were considered to evaluate different pore pressure models.

The Pressure-Dependent Modified Kondner-Zelasko (MKZ) model (Matasović and Vucetic 1993), embedded in DEEPSOIL V7.0, was utilized due to its robustness in capturing nonlinear hysteretic soil behavior under seismic loading to construct site-specific soil models for BH-1 and BH-2 based on soil type and depth. As summarized in Table 1, the uppermost soil unit at all boreholes consists of thick cohesive deposits, which govern the liquefaction and cyclic softening response. Accordingly, detailed liquefaction evaluations were focused on this upper cohesive layer. The model incorporated fundamental and dynamic soil properties, including unit weight (γ), shear wave velocity (V_S), the coefficient of earth pressure at rest (K_0), overconsolidation ratio (OCR), plasticity index (PI), and the minimum damping derived from these parameters (Table 1; Figs. 6 and 7). A maximum transmissible

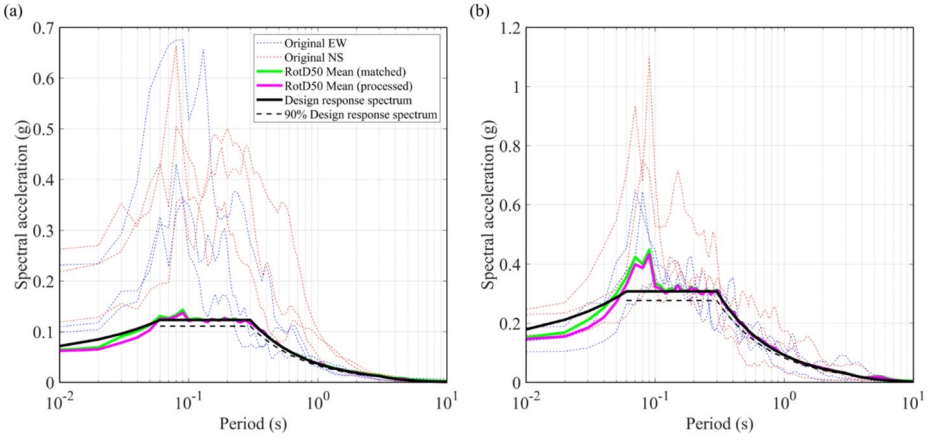

Fig. 5 Comparison of original (dashed), matched (green), and processed (magenta) response spectra of input ground motions for (**a**) service level earthquake (SLE), and (**b**) design basis earthquake (DBE). The target design spectrum (black) and 90% envelope (black dashed) are also shown.</fig>

frequency (f_{max}) of 25 Hz was considered for time-domain nonlinear site response analysis. The V_S profile for site response analysis was determined based on 1-meter interval V_S measurements from geophysical surveys.

For sandy and weathered soil layers, an internal friction angle of 30° was assumed based on nearby design case studies. The K_0 values were estimated using Jáký's equation ($K_0 = 1 - \sin \varphi$) (JAKY 1944). For cohesive soils, K_0 values were calculated using the equation ($K_0 = \nu / (1- \nu)$, where a Poisson's ratio of 0.40 was applied based on adjacent design studies (JAKY 1944). The OCR values were determined from CPT results, applying the mean values per layer while adjusting for depth-dependent decreases. Below the overconsolidated clay layer, the soil was assumed to be normally consolidated, with a minimum OCR value set to 1. The plasticity index (PI) was derived from the difference between the liquid limit (LL) and plastic limit (PL) values from the geotechnical survey report, and the mean value was applied across all clay layers. The D_{min} values were assigned based on the Darendeli (2001) damping curves for each soil layer.

Figure 8 illustrates representative nonlinear curves, including normalized shear modulus reduction and damping curves, developed using the Darendeli (2001) stiffness degradation and damping model. The observed similarity in these curves across different soil layers, particularly for the sand and weathered rock layers (detailed in Figs. 6 and 7), stems from their consistent modeling as predominantly cohesionless material with non-plastic characteristics (PI = 0). This approach reflects the geotechnical survey data, where both layers were classi-

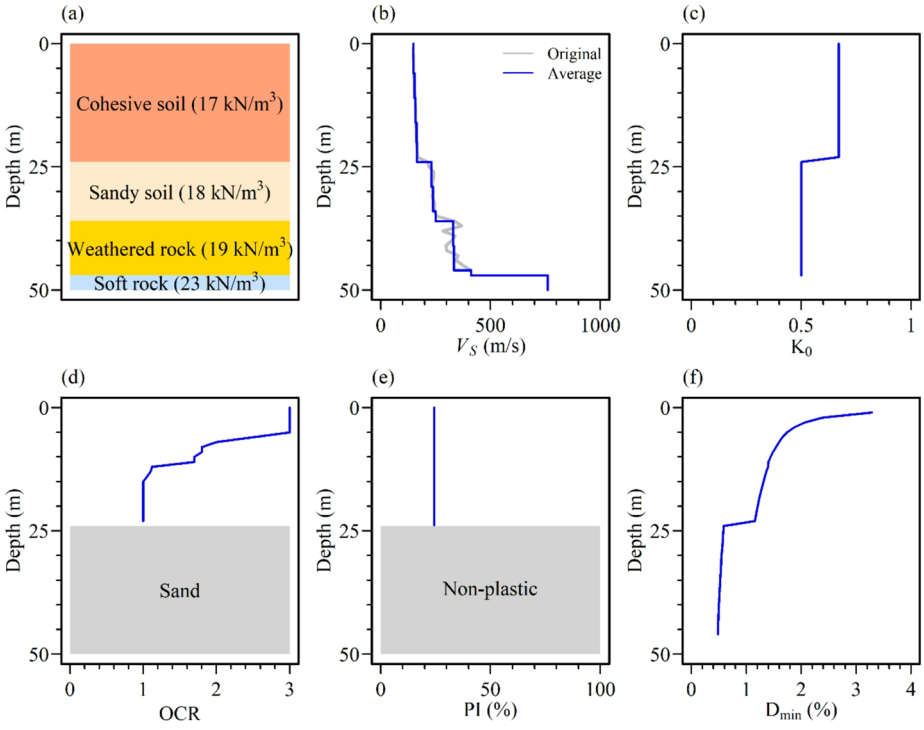

Fig. 6 Depth-dependent input properties for ground response analysis at BH-1: (**a**) unit weight (γ), (**b**) shear wave velocity (V_S), (**c**) coefficient of earth pressore at rest (K_0), (**d**) overconsolidation ratio (OCR), (**e**) plasiticity index (PI), and (**f**) minimum damping ratio (D_{min})

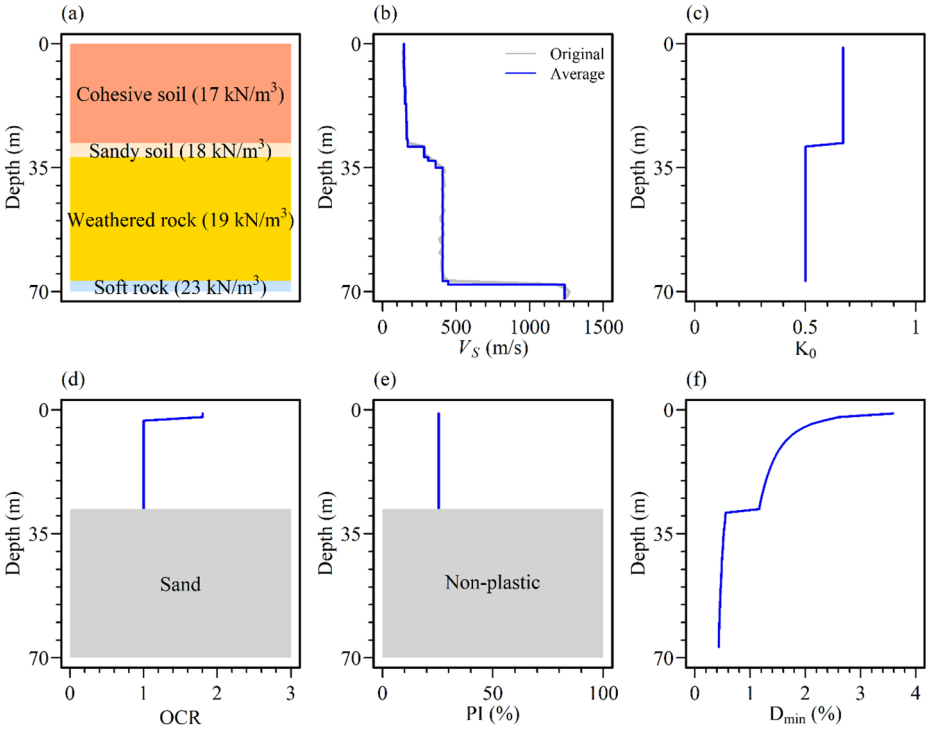

Fig. 7 Depth-dependent input properties for ground response analysis at BH-2: (**a**) unit weight (γ), (**b**) shear wave velocity (V_S), (**c**) coefficient of earth pressore at rest (K_0), (**d**) overconsolidation ratio (OCR), (**e**) plasiticity index (PI), and (**f**) minimum damping ratio (D_{min})

fied as non-plastic and treated as normally or lightly overconsolidated soils. Consequently, this consistent material characterization in comparable small-strain stiffness degradation and damping behaviors is the primary factor, leading to the minimal variations observed in the curves.

The bedrock layer was modeled as an elastic base, where BH-1 was assigned V_S of 760 m/s, γ of 23 kN/m^3, and a damping ratio (ζ) of 0.5%, while BH-2 was assigned V_S of 1,236 m/s, γ of 23 kN/m^3, and ζ of 0.5%. The groundwater level was assumed to be at 0 m for both BH-1 and BH-2. The non-Masing Rule proposed by Phillips and Hashash (2009) was implemented to simulate cyclic soil behavior, while frequency-independent damping was applied for small-strain damping modeling.

Figure 9 presents the acceleration response spectra at the ground surface from both total stress and effective stress-based analyses. The minimal difference between the two spectra indicates that excess pore pressure buildup was limited under the considered seismic loading conditions. This result supports the low liquefaction potential observed in subsequent evaluations and justifies the focus on cyclic softening mechanisms. Furthermore, Fig. 9 also effectively demonstrates the amplification characteristics across different periods. The results indicate that the input rock motions are amplified as they propagate through the soil layers. Notably, the seismic waves exhibit significant amplification within the intermediate-

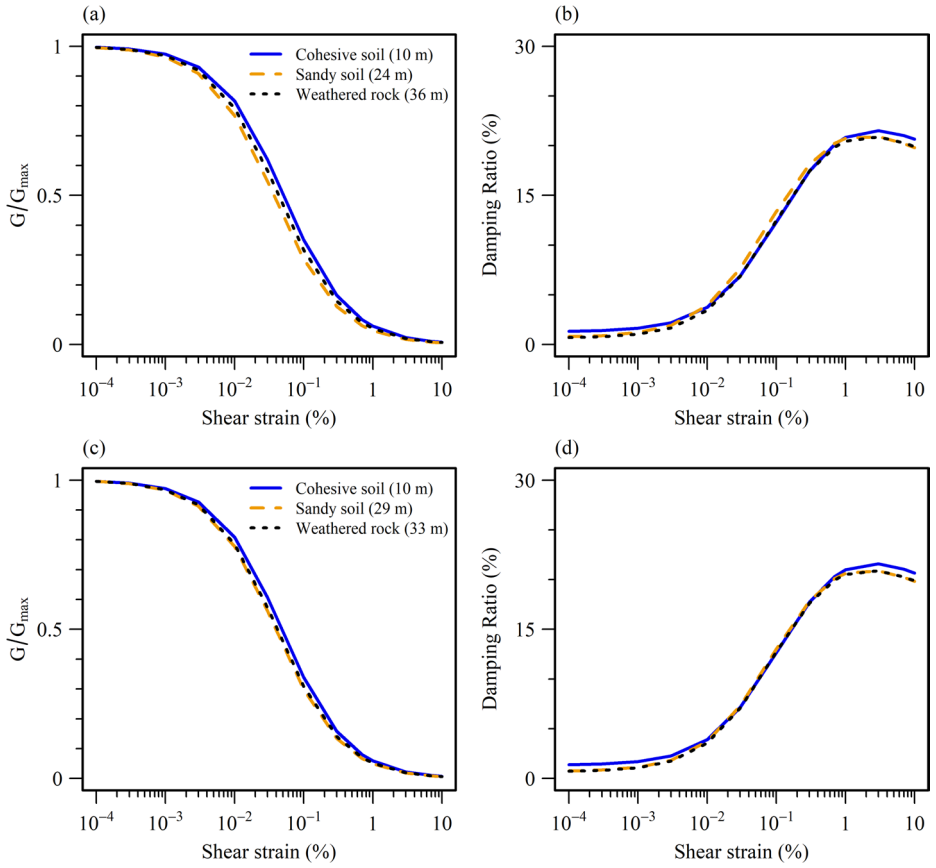

Fig. 8 Nonlinear curves for each soil layer: (**a**) normalized shear moduldus reduction curve at BH-1, (**b**) damping curve at BH-1, (**c**) normalized shear moduldus reduction curve at BH-2, and (**d**) damping curve at BH-2

to-long period range (0.2–2.0 s), which is attributed to the presence of soft clay layers in the subsurface.

5 Assessment of liquefaction

Liquefaction susceptibility assessment is conducted for sandy soil layers within 20 m, where non-cohesive, potentially liquefiable materials are identified based on classification and filed investigation data as the primary scope (ASCE/SEI 7–22, Eurocode 8, KDS 17 10 00). Based on classification and field investigation data, no significant sandy soil layers were identified within this depth range at the study site. Accordingly, the liquefaction potential of the study site was evaluated using the plasticity index (PI), natural water content (*wc*), and liquid limit (LL) obtained from laboratory tests presented in the geotechnical investigation report (Fig. 10; Table 5). The results were compared with the liquefaction susceptibility guidelines for cohesive soils proposed by Bray and Sancio (2006). As the upper

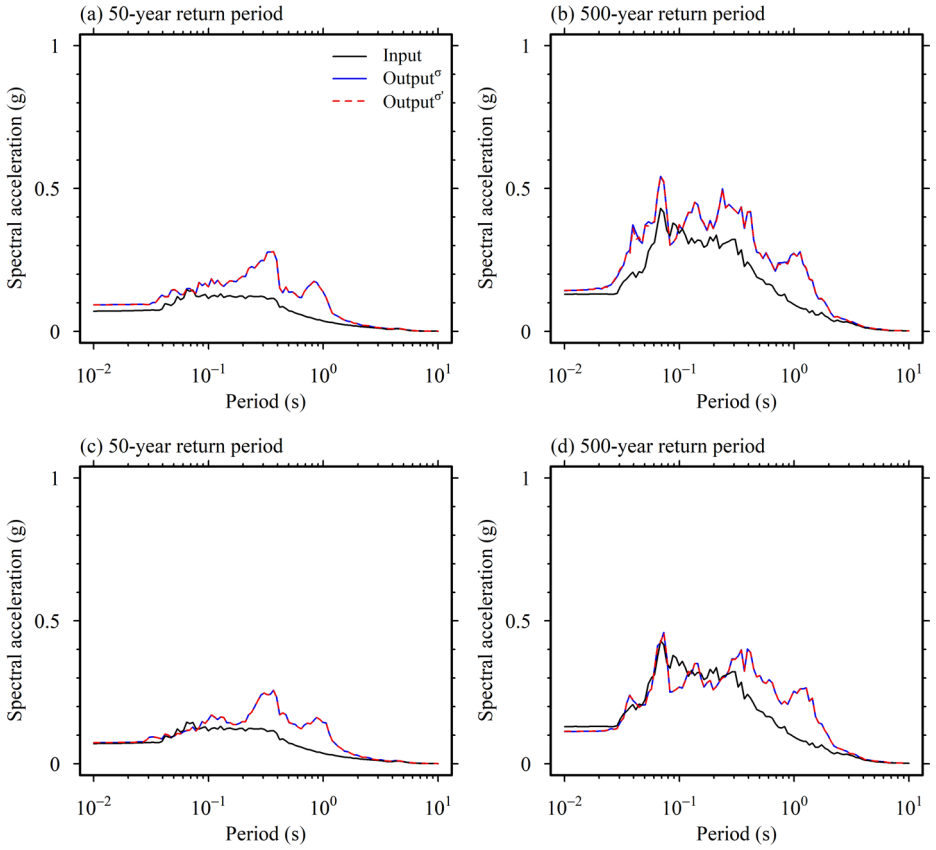

Fig. 9 Acceleration response spectra at the ground surface estimated from input ground motions and analyses using total stress (σ), and effective stress (σ′): (**a**) BH-1–50-year return period ground motion (MKL EW), (**b**) BH-1–500-year return period ground motion (RSN1011 EW), (**c**) BH-2–50-year return period ground motion (MKL EW) (**d**) BH-2–500-year return period ground motion (RSN1011 EW). The black line represents the acceleration response spectrum of the input ground motion, while the blue and red lines indicate the spectra predicted at the ground surface

soil layers of the site consist of highly plastic clay, the likelihood of liquefaction occurrence was determined to be low.

Additionally, the excess pore water pressure (u) and effective stress (σ') obtained from the preceding effective stress analysis were used to compute the excess pore water pressure ratio (R_u) using $R_u = u / \sigma$'. Figure 11 presents the R_u values derived from seismic records corresponding to 50-year and 500-year return periods, where the gray lines represent individual R_u results, and the blue line represents the mean R_u. The criterion for liquefaction occurrence is typically $R_u = 1$. Although R_u values were calculated across all layers, including cohesive soils, interpretation was limited to sand layers due to the inherent limitations of R_u-based criteria in low-permeability and high-plasticity cohesive soils. The maximum mean R_u values estimated for BH-1 and BH-2 were 0.11 and 0.04, respectively, indicating that liquefaction potential at the site is low. This result is consistent with the plasticity-based liquefaction susceptibility assessment.

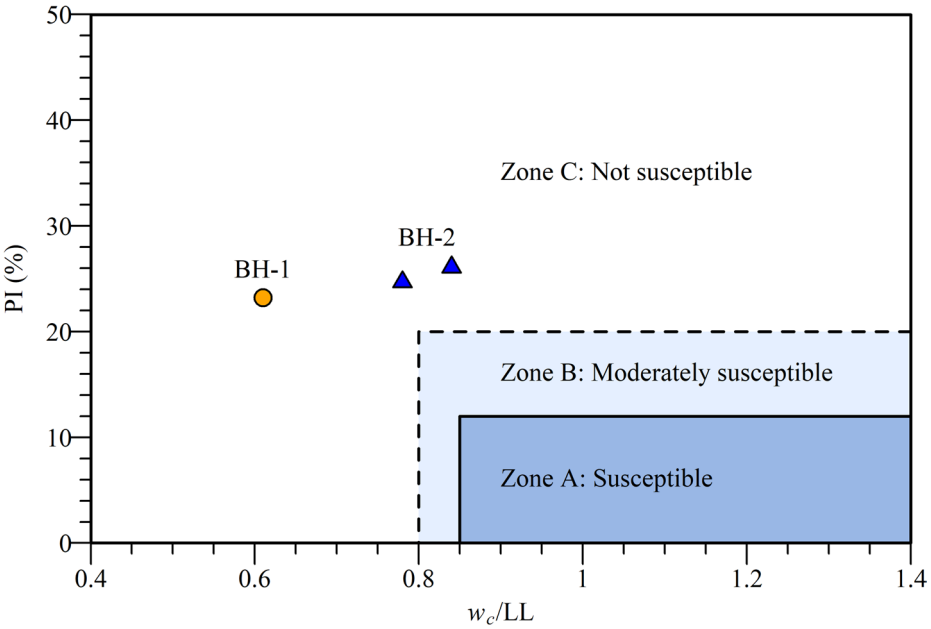

Fig. 10 Liquefaction susceptibility assessment based on plasticity of cohesive soils (Bray and Sancio 2006)

Table 5 Liquefaction susceptibility criteria (Bray and Sancio 2006)

Susceptible	Moderately susceptible	Not susceptible
w_c/LL>0.85 PI≤12	w_c/LL>0.8 12<PI<20	PI>20

To assess the sensitivity of pore water pressure generation, Vucetic and Dobry (1986) and Park and Ahn (2013) models were additionally considered. The subsurface conditions of the study site consist of a thick clay layer extending to approximately 25 m, with a sand layer beneath it. In the sand layer, different pore pressure models resulted in slight variations in excess pore water pressure estimates, but the overall trend remained consistent, confirming the robustness of the effective stress analysis under variable modeling assumptions. However, all pore water pressure (PWP) models consistently produced low R_u values, confirming a low likelihood of liquefaction occurrence.

6 Assessment of cyclic softening potential

To describe the seismic behavior of clay and plastic silt, the term cyclic softening is used, as these soils may experience strength degradation under seismic loading. Therefore, the consideration of cyclic softening is essential in seismic assessments. Cyclic softening susceptibility is evaluated for soils with a behavior type index (I_c) greater than 2.6 (Robertson 1991). The I_c values were calculated incorporating cone tip resistance (q_c), sleeve friction

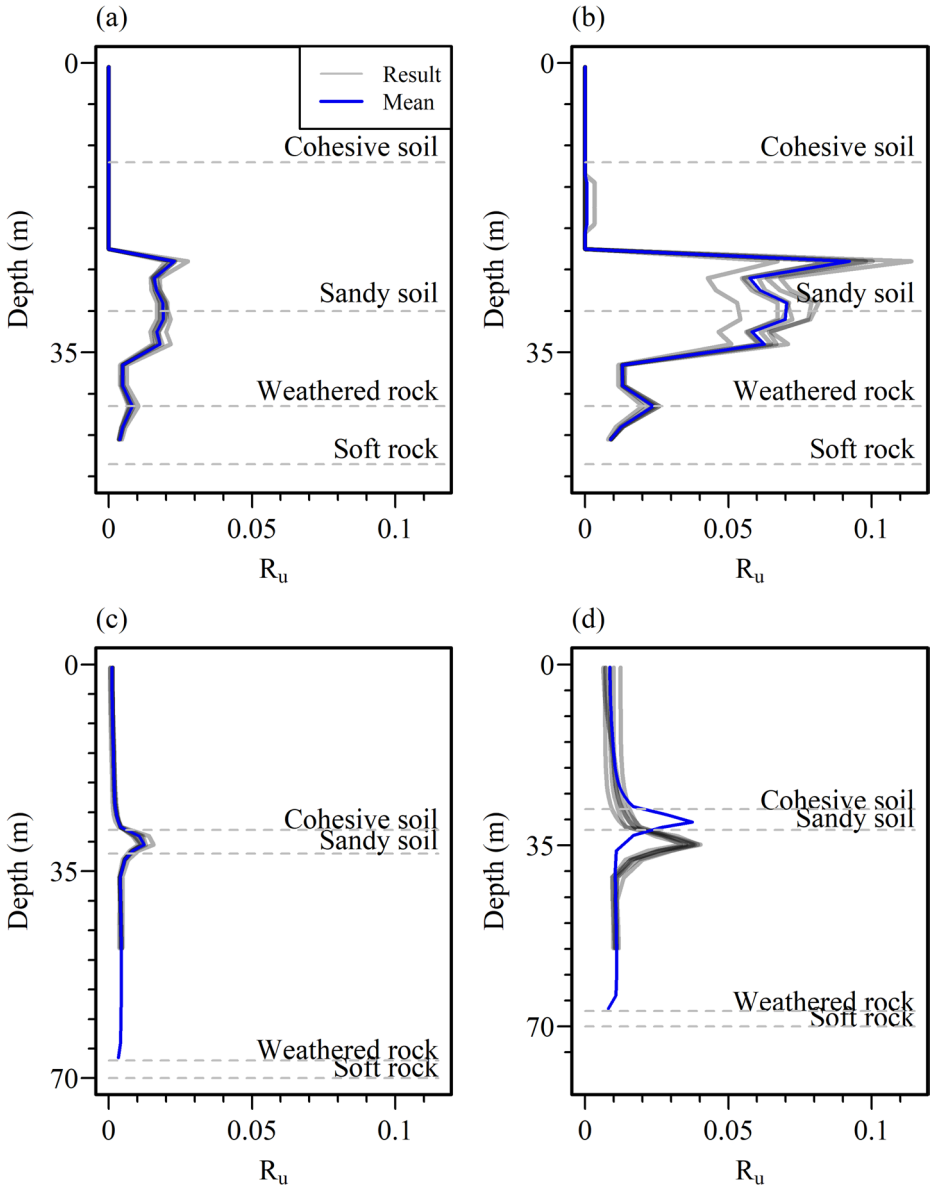

Fig. 11 Depth-averaged excess pore water pressure ratio (R_u): (**a**) BH-1–50-year return period, (**b**) BH-1–500-year return period, (**c**) BH-2–50-year return period, and (**d**) BH-2–500-year return period. The gray lines represent R_u values calculated from six input ground motions, while the blue line indicates the average R_u

(f_s), and excess pore pressure (u_2) obtained from the CPT results documented in the geotechnical investigation report. The cone area ratio (a) was set to 0.8 (Robertson and Fear 1997):

$$I_c = \left[(3.47 - \log Q_t)^2 + (\log F_r + 1.22)^2\right]^{0.5}$$
$$Q_t = \frac{q_t - \sigma}{\sigma'}$$
$$F_r = \frac{f_s}{q_t - \sigma} \times 100\%$$

$$q_t = q_c + u_2 (1 - a) \tag{4}$$

The calculated I_c values for BH-1 and BH-2 were 3.8 and 3.4, respectively, confirming that the site conditions are suitable for cyclic softening assessment. The cyclic softening potential is evaluated based on a factor of safety (FS) threshold of 1, using the equation provided:

$$FS = \frac{CRR \times K_\sigma \times MSF}{CSR} \tag{5}$$

For cyclic stress correction, K_σ was assumed to be 1 (Boulanger and Idriss 2004). The magnitude scaling factor (MSF) was determined based on the method by Boulanger and Idriss (2014):

$$MSF = 1 + (MSF_{max} - 1) \times \left(8.64 \times \exp\left(-\frac{M}{4}\right) - 1.325\right) \tag{6}$$

A moment magnitude of 5 was considered for the 50-year return period, while a moment magnitude of 6.5 was used for the 500-year return period, consistent with the adopted design ground motion levels used in the MSF calculation. For cohesive soils where I_c>2.6, the maximum MSF (MSF_{max}) was set to 1.09, as suggested by Boulanger and Idriss (2014). The cyclic stress ratio (CSR) at various depths was computed incorporating the peak ground acceleration at the surface ($PGA_{surface}$) and the stress reduction factor (r_d) (Idriss 1999; Seed and Idriss 1971):

$$\begin{aligned}
&\mathrm{CSR} = 0.65 \times \frac{\mathrm{PGA_{surface}}}{g} \times \frac{\sigma}{\sigma'} \times r_d \\
&r_d = \exp\left[\alpha(z) + \beta(z) \times M\right] \\
&\alpha(z) = -1.012 - 1.126 \times \sin\left(\frac{z}{11.73} + 5.133\right) \\
&\beta(z) = 0.106 + 0.118 \times \sin\left(\frac{z}{11.28} + 5.142\right)
\end{aligned} \tag{7}$$

In the subsequent CSR calculation, $PGA_{surface}$ was obtained from the site response analysis for each seismic performance level. The adopted PGA values are therefore consistent with the design ground motion levels defined in KDS 17 10 00. The design ground motions were defined from the code-specified response spectrum and implemented through spectrum-matched input records, rather than being taken directly from a regional probabilistic seismic hazard analysis. For offshore conditions, the seabed surface was taken as the reference datum (z=0), and depth z was measured downward from the seabed (Wang et al. 2024;

Qin et al. 2024; Seed and Idriss Izzat 1971). The overlying water column was not explicitly modeled in the CSR evaluation, and vertical stresses were evaluated using the submerged unit weight, so that the effect of seawater was implicitly accounted for through the hydrostatic pore pressure condition at the seabed. The cyclic resistance ratio (CRR) was estimated using undrained shear strength (S_u), as follows:

$$CRR = 0.8 \times \frac{S_u}{\sigma'} \times K_\alpha \tag{8}$$

The static shear stress correction factor (K_α) was set to 1, assuming a level ground condition with no structural loads (Boulanger and Idriss 2014, 2007). Due to the uncertainty in S_u values, in addition to the measured values from site investigations, alternative estimates were computed following the equation (Table 6):

$$S_u = \begin{cases} 0.06 \times (N)_{60} \times P_a & for\ SPT \\ \frac{q_c - \sigma}{N_k} & for\ CPT \end{cases} \tag{9}$$

The corrected SPT blow count ($(N)_{60}$) was derived from the raw N values, assuming a 60% energy efficiency. The atmospheric pressure (P_a) was set to 101.3 kPa, and for marine clay layers, the overburden correction factor (N_k) was assumed to be 20 (Jörß 1998). For the upper cohesive unit (approximately 0–20 m), the CPT-based S_u was estimated using a representative q_c value reported for this layer in the investigation report, given the relatively uniform cone resistance profile. Accordingly, S_u (and the resulting CRR) from the CPT-based approach is treated as a layer-representative value for this interval, while depth-dependent trends are evaluated using the 1 m interval calculations based on SPT-derived parameters. The S_u values estimated from SPT- and CPT-based correlations represent field-equivalent undrained shear strength commonly adopted in simplified cyclic softening evaluations for cohesive soils. The S_u/σ′-based CRR formulation is intended to represent the initiation of cyclic strength degradation under seismic loading and is consistent with simplified cyclic softening evaluations for cohesive soils. This formulation does not imply strict strain compatibility with peak cyclic shear strains, but rather provides a simplified index for the onset of cyclic strength degradation under seismic loading. Accordingly, the adopted approach provides a rational basis for screening cyclic softening susceptibility and for comparative evaluation of sensitivity to seismic demand. For BH-1, the layer-representative CRR values obtained from CPT- and SPT-based approaches are 0.12 and 0.09, respectively, indicating a comparable magnitude of cyclic resistance for the upper cohesive unit despite differences in the underlying correlations.

The factor of safety (FS) for cyclic softening was calculated at each depth using three different S_u estimation methods. This approach allows for comparison between SPT- and CPT-based CRR estimates and highlights the sensitivity of cyclic softening assessment to

Table 6 Undrained shear strength (S_u, kPa) derived from exploration, SPT, and CPT results

Borehole ID	Exploration-based results	SPT-based results	CPT-based results
BH-1	16.1	10	12.8
BH-2	16.5	10	14.1

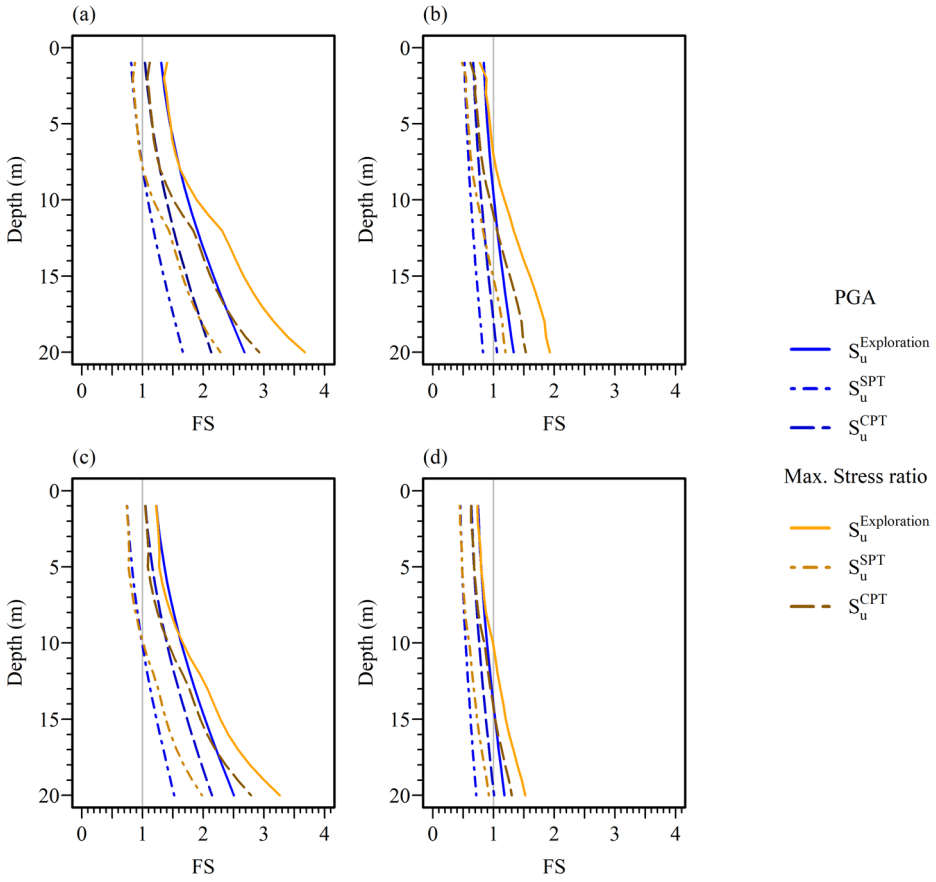

Fig. 12 Factor of safety (FS) against cyclic softening estimated using S_u obtained from exploration, SPT, and CPT results: (**a**) BH-1–50-year return period, (**b**) BH-1–500-year return period, (**c**) BH-2–50-year return period, and (**d**) BH-2–500-year return period. The values represent the average FS across all input ground motions

the choice of in-situ test interpretation. Figure 12 illustrates the mean FS values for the seismic records corresponding to the 50-year and 500-year return periods. At BH-1, the FS results indicate generally low cyclic softening potential at shallow depths for the 50-year return period (FS > 1), while for the 500-year return period, cyclic softening potential was high across all depths. This indicates potential for strain accumulation or strength degradation under seismic loading, which must be considered in foundation design to ensure serviceability. At BH-2, cyclic softening potential was found to be low for the 50-year return period, whereas it was generally high for the 500-year return period. The FS values varied depending on the S_u estimation method, indicating the sensitivity of cyclic softening potential to the choice of undrained shear strength. Despite differences in absolute FS values, the depth-dependent trends of cyclic softening potential were generally consistent across the different S_u estimation methods, and were comparable between BH-1 and BH-2. Without a clear consensus on the most appropriate estimation method for this site, the range of FS results is presented to reflect the inherent uncertainty in cohesive soil behavior.

The factor of safety computed using the maximum shear stress values obtained from the site response analysis, as outlined in KDS 17 10 00, is presented in Fig. 12. The FS results obtained from this method were slightly higher than those computed using the stress reduction factor, confirming the robustness of the applied methodology. Overall, the results emphasize the need to incorporate cyclic softening assessments into seismic design for offshore foundations, particularly in cohesive soil conditions, and highlight the importance of refining S_u estimation methods through further site-specific investigations.

7 Discussion and conclusion

The results of this study indicate that the seismic performance of offshore platforms founded on cohesive seabed soils may be governed by cyclic softening-induced deformation rather than liquefaction triggering. Although conventional liquefaction evaluation methods suggest stability at the investigated site, the analyses reveal that the margin of safety is relatively limited and highly sensitive to seismic demand. In particular, a moderate increase in design earthquake level leads to a pronounced increase in cyclic stress ratio and cyclic softening potential, even when liquefaction criteria are satisfied. From an offshore foundation design perspective, this finding underscores the importance of considering deformation-related mechanisms and serviceability requirements, rather than relying solely on liquefaction triggering as a pass-fail criterion.

This study conducted site response analysis and liquefaction assessment for the offshore demonstration site (BH-1, BH-2) to derive the following key findings:

1. Site Response Analysis: Based on previously conducted in-situ geotechnical investigations, soil properties were quantified, and nonlinear site response analysis was performed. The results indicated significant amplification of seismic waves in the 0.2–2.0 s period range, attributed to the presence of soft clay layers.
2. Liquefaction Assessment: The liquefaction potential of BH-1 and BH-2 was evaluated based on the Korean seismic design standard (KDS 17 10 00), relevant studies, and effective stress analysis. The high-plasticity clay layers identified at both sites suggest a low susceptibility to liquefaction.
3. Cyclic Softening Evaluation: The potential for cyclic softening was assessed using international methodologies. The evaluation revealed that cyclic softening could occur at shallow depths under 50-year return period seismic motions, while it could affect the entire depth range under 500-year return period seismic motions. However, the FS varies significantly depending on the method used to calculate *Su* values, highlighting the sensitivity of cyclic softening assessments to input assumptions.

Although the individual analyses indicate that the target site remains stable against liquefaction under design-level seismic motions, the comparison between different return-period ground motions demonstrates that the cyclic stress ratio and softening potential increase rapidly with increasing seismic demand, highlighting the limited safety margin in the cohesive soils considered.

Overall, the findings confirm that the target site is stable against liquefaction for offshore structural design under design-level seismic motions. However, the analyses also demon-

strate that stability is achieved with a relatively narrow safety margin, and that the potential for cyclic softening increases rapidly as seismic demand intensifies. Therefore, seismic assessment of subsea foundations should not rely solely on liquefaction triggering criteria, but should also consider deformation-related mechanisms and their sensitivity to design assumptions.

The reliability of the liquefaction evaluation method adopted in this study is supported by previous research in South Korea, where similar methodologies have been validated against documented liquefaction cases (Cho et al. 2024; Seo et al. 2024). While these previous studies primarily focused on onshore case histories where liquefaction or cyclic softening was clearly observed, the present study addresses a complementary condition in which standard evaluation methods indicate stability, yet with limited safety margins relevant to offshore platform design.

Furthermore, the assessment framework employed in this study aligns with international liquefaction evaluation standards, such as ASCE 7, Eurocode 8, and other global seismic design guidelines. This confirms that the applied methodology is not only suitable for Korean offshore geotechnical conditions but also compatible with internationally recognized seismic hazard assessment practices.

Some limitations should be acknowledged. Although the adopted methodology has been validated for onshore and nearshore environments, direct offshore observations of liquefaction and cyclic softening remain limited. In addition, uncertainties associated with empirical correlations for undrained shear strength, fines content corrections, and seismic demand parameters may influence the predicted cyclic resistance and stress ratios. For example, alternative S_u correlations, fines correction methods, or changes in magnitude scaling factors and input PGA values could affect the computed factor of safety. While a formal probabilistic or sensitivity analysis is beyond the scope of this study, such uncertainties should be considered when interpreting factor-of-safety values close to unity and when applying the results for design-level decision making.

Author Contributions All authors contributed to the study conception and design. Material preparation, data collection, and analysis were performed by Jieun Kim, Hyung-Ik Cho, and Jae-Hyun Kim. The original draft of the manuscript was written by Hyejin Lee. Conceptualization, methocdology development, and visualization were led by Hyejin Lee with contributions from Byungmin Kim. Supervision and overall guidance were provided by Taek Hee Han. Funding acquisition and project administration were managed by Taek Hee Han, Jun Kil Park, and Youngjin Choi. Jeongmin Goo supported project coordination and resource management. All authors reviewed and approved the final manuscript.

Funding Open Access funding enabled and organized by Seoul National University. This research was supported by the Korea Institute of Marine Science & Technology Promotion (KIMST), funded by the Ministry of Oceans and Fisheries (RS-2022-KS221606).

Data availability The datasets generated during the current study are available from the corresponding author on reasonable request.

Declarations

Competing interests The authors have no relevant financial or non-financial interests to disclose.

References

Ahn J-K, Baek W-H, Choi J-S, Kwak DY (2018) Investigation of Pohang earthquake liquefaction using 1D effective-stress site response analysis. J Korean Geotech Soc 34(8):37–49

Al Atik L, Abrahamson N (2010) An Improved Method for Nonstationary Spectral Matching. Earthq Spectra 26(3):601–617. https://doi.org/10.1193/1.3459159

American Society of Civil Engineers (ASCE) (2022) Minimum design loads and associated criteria for buildings and other structures. American Society of Civil Engineers

Boore DM (2010) Orientation-Independent, Nongeometric-Mean Measures of Seismic Intensity from Two Horizontal Components of Motion. Bull Seismol Soc Am 100(4):1830–1835. https://doi.org/10.1785/0120090400

Boulanger RW, Idriss IM (2004) Evaluating the potential for liquefaction or cyclic failure of silts and clays

Boulanger RW, Idriss IM (2007) Evaluation of cyclic softening in silts and clays. J Geotech Geoenviron Eng 133(6):641–65

Boulanger RW, Idriss IM (2014) CPT and SPT based liquefaction triggering procedures. Report No. UCD/CGM.-14 1:134

Bray JD, Sancio RB (2006) Assessment of the liquefaction susceptibility of fine-grained soils. J Geotech GeoEnviron Eng 132(9):1165–1177

Cho Y, Han JT, Choo YW, Lee J, Kim J, Kim K, Park K-h, Kim J-H, Park H-J, Kwak D, Park D, Choi J-S, Kim S-R, Kim B (2024) Assessments of Liquefaction Triggering Using In Situ and Laboratory Tests in Pohang, South Korea. J Geotech GeoEnviron Eng 150(12):04024132. https://doi.org/10.1061/JGGEFK.GTENG-12135

Darendeli MB (2001) Development of a new family of normalized modulus reduction and material damping curves. The university of Texas at Austin

Gihm YS, Kim SW, Ko K, Choi J-H, Bae H, Hong PS, Lee Y, Lee H, Jin K, Choi S (2018) Paleoseismological implications of liquefaction-induced structures caused by the 2017 Pohang earthquake. Geosci J 22(6):871–880

Green R, Mitchell J, Polito C (2000) An energy-based excess pore pressure generation model for cohesionless soils in Proceedings of the John Booker Memorial Symposium, Sidney Australia, AA Balkema Publishers, Rotterdam, Netherlands. Citeseer

Han TH, Yi J-H, Han S-H, Won D, Park W-S (2013) Key Technologies for Construction of Seabed Base. J Korean Soc Hazard Mitig 13(3):215–226

Han TH, Hong H, Kim S (2021) Trends and Plans of Subsea Space Creation and Utilization Technology in Proceedings of the Korean Institute of Navigation and Port Research Conference. Korean Institute of Navigation and Port Research:89–90

Hong T-K, Park S, Lee J, Lee J, Kim B (2024) Middle to lower crustal earthquakes in the western East Sea (Sea of Japan) and their implications for neotectonic evolution. Tectonophysics 880:230346. https://doi.org/10.1016/j.tecto.2024.230346

Huang Y, Han X (2020) Features of Earthquake-Induced Seabed Liquefaction and Mitigation Strategies of Novel Marine Structures. J Mar Sci Eng 8(5):310

Idriss I (1999) An update to the Seed-Idriss simplified procedure for evaluating liquefaction potential. Proc., TRB Worshop on New Approaches to Liquefaction, Pubbl. n. FHWA-RD-99-165, Federal Highway Administation

JAKY J (1944) The coefficient of earth pressure at rest. Journal of the Society of Hungarian Architects and engineers

Jeng D-S (2015) Review of Liquefaction Around Marine Structures by B. Mutlu Sumer. J Waterw Port Coast Ocean Eng 141(5):07515001. https://doi.org/10.1061/(ASCE)WW.1943-5460.0000296

Jörß O (1998) Erfahrungen bei der Ermittlung von cu-Werten mit der Hilfe von Drucksondierungen in bindigen Böden. geotechnik 21(1):26–27

Kang S, Kim B, Bae S, Lee H, Kim M (2019) Earthquake-Induced Ground Deformations in the Low-Seismicity Region: A Case of the 2017 M5.4 Pohang, South Korea, Earthquake. Earthq Spectra 35(3):1235–1260. https://doi.org/10.1193/062318eqs160m

KDS 17 10 00 (2024) Korean seismic design code I a T Ministry of Land (Editor), Sejong, South Korea
KDS 64 17 00 (2019) Korean Design Standard: Seismic design M o O a Fisheries (Editor), Sejong, South Korea
Kim J, Kim B, Cho H (2020) Shear Wave Velocity Estimation in Korea Using P-Wave Seismograms. KSCE J Civ Eng 24(12):3650–3658. https://doi.org/10.1007/s12205-020-0752-4
Kim H-S, Kim M, Baise LG, Kim B (2021) Local and regional evaluation of liquefaction potential index and liquefaction severity number for liquefaction-induced sand boils in Pohang, South Korea. Soil Dyn Earthq Eng 141:106459
Kim CH, Kim K-H, Choi SY, Kim WH, Choi HO, Park CH (2022a) Gravity and magnetic anomalies of earthquake-prone areas in the southwestern Ulleung basin margin, East Sea (Sea of Japan). Sci Rep 12(1):17172. https://doi.org/10.1038/s41598-022-21462-3
Kim K, Kim H, Kim S-R, Lee J (2022b) Verification of the Seismic Performance Evaluation Methods for Enclosure Dam. J Korean Geotech Soc 38(5):19–33
Korea Meteorological Administration (KMA) (2012) Historical Earthquake Records in Korea (2∼1904). Korea Meteorological Administration, Seoul, South Korea
Kumagai T, Yanagibashi T, Tsutsumi A, Konishi C, Ueno K (2020) Efficient surface wave method for investigation of the seabed. Soils Found 60(3):648–667. https://doi.org/10.1016/j.sandf.2020.04.005
Kuo Y-S, Weng T-L, Hsu H-T, Chang H-W, Lin Y-C, Chang S-C, Chuang Y-J, Tseng Y-H, Wong Y-T (2021) A Methodology for Estimating the Position of the Engineering Bedrock for Offshore Wind Farm Seismic Demand in Taiwan. Energies 14(9):2474
Kyung J-B (2010) Paleoseismological study and evaluation of maximum earthquake magnitude along the Yangsan and Ulsan Fault Zones in the Southeastern Part of Korea. Geophys Geophys Explor 13(3):187–197
Lee GH (1998) Historical earthquake data of Korean. J Korean Geophys Soc 1(1):3–22
Lee H, KIM J, Ko K, Gihm Y, Kim J, Lee S (2018) Characteristics of sand volcanoes caused by 2017 Pohang Earthquake-induced liquefaction and their paleoseismological approach. J Geol Soc Korea 54(3):221–235
Lee M-G, Kim Y, Cho H-I, Kim H-S, Sun C-G, Seong Y-J, Che I-Y (2024) KIGAM quake: An open platform for seismological data and earthquake research information. Geomech Eng 37(3):279
Matasović N, Vucetic M (1993) Cyclic characterization of liquefiable sands. J Geotech Eng 119(11):1805–1822
Matasović N, Vucetic M (1995) Generalized Cyclic-Degradation-Pore-Pressure Generation Model for Clays. J Geotech Eng 121(1):33–42. https://doi.org/10.1061/(ASCE)0733-9410(1995)121:1(33)
Microsoft (2025) Available at: https://natick.research.microsoft.com/
Ministry of Land, Infrastructure and Trasport (MOLIT) and Korea Authority of Land & Infrastructure Safety (2021) Existing Building Seismic Performance Evaluation Guidelines
Ministry of Construction and Transportation (1997) A Study on Site-Specific Seismic Design Response Spectrum
National Emergency Management Agency (2013) National Seismic Hazard Map of Korea, South Korea
National Oceanic and Atmospheric Administration (NOAA) (2025) Available at: https://oceanexplorer.noaa.gov/projects/02aquarius/aquarius.html
Park D, Ahn JK (2013) Accumulated stress based model for prediction of residual pore pressure. Proceedings of the 18th international conference on soil mechanics and geotechnical engineering 2:1567–70
Phillips C, Hashash YM (2009) Damping formulation for nonlinear 1D site response analyses. Soil Dyn Earthq Eng 29(7):1143–1158
Qin X, Yang Z, Cui Y, Liu X, Tian H, Guo L, Ling X (2024) Spatial distribution characteristics of soil liquefaction potential in the Yellow River Subaquatic Delta, China. Mar Georesources Geotechnology 42(4):420–431. https://doi.org/10.1080/1064119X.2023.2194876
Robertson P (1991) Soil classification using the cone penetration test: Reply. Can Geotech J 28(1):176–178
Robertson PK, Fear C (1997) Cyclic liquefaction and its evaluation based on the SPT and CPT in Proceeding of the NCEER workshop on evaluation of liquefaction resistance of soils:41–87
Seed HB, Idriss IM (1971) Simplified procedure for evaluating soil liquefaction potential. J Soil Mech Found Div 97(9):1249–1273
Seed HB, Idriss Izzat M (1971) Simplified Procedure for Evaluating Soil Liquefaction Potential. J Soil Mech Found Div 97(9):1249–1273. https://doi.org/10.1061/JSFEAQ.0001662
Seismosoft (2020) Available at: www.seismosoft.com
Seo J-M, Choi I-K (1998) Estimation of magnitude of historical earthquakes considering earthquake characteristics and aging of a house. J Earthq Eng Soc Korea 2(4):1–11
Seo H, Kim H-S, Baise LG, Kim B (2024) Geospatial liquefaction probability models based on sand boils occurred during the 2017 M5. 5 Pohang, South Korea, earthquake. Eng Geol 329:107407

Shi W, Cai G, He H, Liu X, Yu S, Zhang G, Liu F, Li M, Liu S (2025) Apparent aging of seabed sediments and its implications on liquefaction assessment: a case study of Jintang strait. Acta Geotech. https://doi.org/10.1007/s11440-025-02855-w

Standard B (2005) Eurocode 8: Design of structures for earthquake resistance. Part 1:1998–1991

Sun C-G, Cho H-I, Kim H-S, Lee M-G (2022) Determining N value from SPT blows for 30 cm penetration in weathered strata. Geomech Eng 28(6):625–636

Tian H, Chen L (2021) Research on Assessment of Earthquake Liquefaction in Offshore Wind Turbine Based on Dynamic Triaxial Test in *2021 7th International Conference on Hydraulic and Civil Engineering & Smart Water Conservancy and Intelligent Disaster Reduction Forum (ICHCE & SWIDR)*:1131–1138

Tsai C-C, Kishida T, Kuo C-H (2019) Unified correlation between SPT–N and shear wave velocity for a wide range of soil types considering strain-dependent behavior. Soil Dyn Earthq Eng 126:105783. https://doi.org/10.1016/j.soildyn.2019.105783

Venkataramana K, Kawano K (1995) Nonlinear dynamics of offshore structures under sea wave and earthquake forces. Sadhana 20(2):501–512. https://doi.org/10.1007/BF02823205

Vucetic M, Dobry R (1986) Pore pressure build-up and liquefaction at level sandy sites during earthquakes. Rensselaer Polytechnic Institute Research Report. CE-86–3

Wang Y, Guo X, Liu J, Hou F, Zhang H, Gao H, Liu X (2024) A Methodology for Susceptibility Assessment of Wave-Induced Seabed Liquefaction in Silt-Dominated Nearshore Environments. J Mar Sci Eng 12(5):785

Authors and Affiliations

Hyejin Lee[1,2] · Byungmin Kim[3] · Jieun Kim[3] · Taek Hee Han[1] · Jun Kil Park[1] · Youngjin Choi[1] · Hyung-Ik Cho[4] · Jae-Hyun Kim[5] · Jeongmin Goo[6]

✉ Hyejin Lee
hyejin.lee@snu.ac.kr; hyejinee517@gmail.com

[1] Ocean Space Development and Energy Research Department, Korea Institute of Ocean Science and Technology, 385, Haeyang-ro, Yeongdo-gu, Busan 49112, Republic of Korea

[2] Gyeonggi Disaster and Safety Research Center, Advanced Institute of Convergence Technology (AICT), Seoul National University, 145 Gwanggyo-ro, Suwon 16229, Republic of Korea

[3] Department of Civil, Urban, Earth, and Environmental Engineering, Ulsan National Institute of Science and Technology (UNIST), 50 UNIST-gil, Eonyang-eup, Ulju-gun, Ulsan 44919, South Korea

[4] School of Civil, Environmental & Architectural Engineering, Gyeongkuk National University, Andong 36729, Republic of Korea

[5] Department of Civil Engineering, Kangwon National University, Chuncheon-si, Gangwon- do 24341, Republic of Korea

[6] Research and Development Center, Dong Myeong Engineering Consultants, DM Square, 35 Godeok Biz Valley-ro 4-gil, Gangdong-gu, Seoul, Republic of Korea